


Sensory carbon fiber based textile-reinforced concrete for smart structures

Journal of Intelligent Material Systems and Structures
2016, Vol. 27(4) 469–489
© The Author(s) 2015
Reprints and permissions:
sagepub.co.uk/journalsPermissions.nav
DOI: 10.1177/1045389X15571385
jim.sagepub.com


Yiska Goldfeld¹, Oded Rabinovitch¹, Barak Fishbain¹, Till Quadflieg² and Thomas Gries²

Abstract

This article investigates the feasibility of intelligent textile-reinforced concrete structural elements with sensing capabilities. The concept is based on dual use of glass and carbon fiber textiles as reinforcement and, at the same time, as a sensory agent. Experimental investigation demonstrates the feasibility of the concept in two applications: detecting strains in a mechanically loaded textile-reinforced concrete beam and monitoring the interaction of the structural element with a wet environment. By detecting the changes to the integrative electrical resistance of the carbon tow, the ability of the textile to sense strain and exposure to water is demonstrated. For strain sensing, the hybrid reinforcing textile provides electro-mechanical sensing with a gauge factor of the order of 1 and a detectable correlation with the load, strain, and displacement responses. For the detection of wetting, the implementation of the carbon tow in a Wheatstone bridge detects fractional resistance changes in the order of 10^{-5} , a figure that is effectively detected by monitoring the voltage across the bridge. The response to wetting, which is conditioned by the cracking of the beam and the exposure to ionic conductive solutions, provides a mean to monitor the functionality and the structural health of the textile-reinforced concrete beam.

Keywords

Textile-reinforced concrete, structural health monitoring, sensing, signal processing, intelligent structures, carbon fibers, structural mechanics

Introduction

The development of intelligent concrete structures is one of the most challenging frontiers of today's structural engineering. It is a key towards to a significant and meaningful reduction in consumption of natural materials, the mitigation of construction impact on the environment, and the development of effective and safe lightweight concrete structures. On a larger scale, it is a fundamental element in development of intelligent urban environments that can sense and quantify the impact of catastrophic events such as earthquakes, tsunamis, storms, or acts of terror. Such intelligent urban environment will be able to assess the residual strength of structures or even guide the allocation of medical and rescue response teams.

Tomorrow's intelligent structures will combine high-performance material and structural systems, structural health monitoring systems, and functionality monitoring systems. Instead of joining three separate systems (i.e. the structural system, the health monitoring system, and the functionality monitoring system) in one

element, tomorrow's intelligent structure will be a multifunctional element that addresses the three tasks at once. This study faces this challenge and looks at the feasibility of a textile-reinforced concrete (TRC) structural element with self-sensing capabilities.

Carbon fiber reinforcement is characterized by its high specific strength and corrosion resistance. These features make it perfectly suitable for the use in various types of TRC structural components (Berger et al., 2011). Production methods of TRC components include laminating, casting, spraying, spinning, and injection molding. In the TRC industry, glass fiber reinforcement materials are the main reinforcement

¹Faculty of Civil and Environmental Engineering, Technion – Israel Institute of Technology, Haifa, Israel

²Institut für Textiltechnik, RWTH Aachen University, Aachen, Germany

Corresponding author:

Yiska Goldfeld, Faculty of Civil and Environmental Engineering, Technion – Israel Institute of Technology, Technion City, Haifa 32000, Israel.
Email: yiska@tx.technion.ac.il

medium, whereas carbon fiber materials are embedded in the main reinforcement layers. By optimizing the arrangement of the carbon tows in the glass fiber-based textile, cost-effective structures are achievable (Hegger et al., 2011). One attractive application of TRC is found in the field of pipes and tanks (Franzke et al., 2005; Lieboldt et al., 2006). In this case, the use of textile reinforcement can easily follow the curved geometry and improve the constructability. It also allows the reduction in wall thickness, mainly due to the superior corrosion resistance of the reinforcement materials. Applications such as pipelines for drinking water or wastewater as well as water tanks are inherently susceptible to leakage due to concrete cracking. Therefore, they become a natural candidate to the application of a structural system that combines strength and stiffness with structural health and functionality monitoring capabilities.

Monitoring techniques for reinforced concrete (RC) elements range from traditional ones such as visual inspection or tap tests, to modern techniques based on embedded or surface-mounted strain sensors. The latter are either localized such as resistor strain gauges and fiber Bragg grating or distributed such as time domain reflectometry in fiber optics. In the field of strain sensing with fiber optics, Majumder et al. (2008), Li et al. (2004), and Lee (2003) presented reviews of the sensory application of fiber Bragg gratings and fiber optic sensors to structural health monitoring in civil engineering. Khotiaintsev et al. (2013) compared several types of optical fibers embedded in concrete beam specimens and highlight the challenges of the technology.

In the context of the sensory TRC elements, a range of research works reported on the implementation of sensory fiber optics as well as other sensors in the textile mesh. For example, Montanini et al. (2012) installed Bragg grating-based fiber optic sensors in a woven polyparaphenylene benzobisoxazole (PBO) bidirectional ($0^\circ/90^\circ$) mesh and compared the strain readings with those of conventional strain gauges. Krebber et al. (2012) also used textiles in order to deploy optical time domain reflectometry (OTDR) and Brillouin optical time domain reflectometry (BOTDR) for geotechnical applications as well as for strengthened masonry structures. The BOTDR technique is a promising direction in this field, mainly due to its ability to identify and quantify locally damaged regions such as local cracks (Goldfeld and Klar, 2013; Klar et al., 2010). Quadflieg et al. (2013) and later Goldfeld et al. (2014) focused on the development of sensory TRC elements and embedded metallic yarns in the reinforcing textile for sensing strain and humidity. The implementation of the metallic wires and the types of wires used in Quadflieg et al. (2013) and Goldfeld et al. (2014) aimed at providing the system with the sensory capacity but without any significant contribution to the load-carrying system.

The methods discussed above are all based on the implementation of a sensing system in a structural element. The physical accommodation in the load-bearing element, the potential degradation of the effective properties of the host element, and the clear distinction between the structural system and the sensory one (which is not a part of the load-bearing system) are drawbacks of these approaches. Stemming from the concept of joining two separate systems together, the interface between the structural and the sensory systems and the corresponding ability to maintain a coordinated action of the two are also potential weak aspects. Finally, the sensory system itself is commonly expansive and its implementation is costly, time-consuming, and it requires specially trained personnel. In the light of these drawbacks, this study aims at taking advantage of the favorable features of the TRC technique and investigates the feasibility of a TRC element with a self-sensing capability.

Many of the studies that examined the use of carbon fibers for sensing in concrete structures focused on short carbon fibers randomly mixed in the concrete mixture, see, for example, Chen and Chung (1993a, 1993b, 1995), Chung (2000a, 2000b, 2001a, 2002, 2003, 2005), Wen and Chung (2005, 2007), Xu and Chung (2001), Meehan et al. (2010), McCarter et al. (2007), Vaidya and Allouche (2011), and Ding et al. (2013). The mixing of the short carbon fibers improves the electrical conductivity of the casted concrete element with a distinction between fibers content above the percolation threshold (where the fibers touch each other and form a continuous electrically conductive path) and fiber content below that threshold; see Wen and Chung (2008). The changes to the electrical properties due to the changes to the structural health state in the form of straining can then be electrically measured and monitored through the piezoresistive effect. The pioneering works of Chen and Chung (1993a, 1993b, 1995) explored this effect and investigated the development of carbon fiber RC elements with the abilities of strain sensing and micro-cracking detection. Wen and Chung (2006) investigated the effect of embedded steel reinforcing bars on the piezoresistivity of the short carbon fibers mixed in the concrete, and Wen and Chung (2008) investigated the effect of moisture on the piezoresistivity of cement paste with mixed carbon fibers below the percolation threshold. Later, Han et al. (2007) and Ou and Han (2009) took another step toward the self-sensory concept and developed a sensor that is based on a piezoresistive material made of short carbon fibers and cement paste. A detailed review of the broad spectrum of studies on cement-matrix composites for sensory and smart structures is presented in Chung (2000a, 2000b, 2012).

Vaidya and Allouche (2011) investigated the possibility of using carbon-based conductive geopolymer in concrete structures as smart material for health

monitoring application. Ding et al. (2013) studied the effect of the types of the carbon fibers on the mechanical properties and on the fractional change in resistance of the entire concrete element. In these studies, the concept was based on short carbon fibers that were added to the concrete mixture. The randomly distributed carbon fibers dictate the macroscopic electro-mechanical properties of the concrete element. Electrically connecting the element using surface-mounted electrodes or conductive adhesive tapes attached to the surface of the element and monitoring the electro-mechanical properties and their changes with the structural state set the basis for the sensory feature.

A different sensing concept is based on the detection of changes to the electrical resistance of continuous carbon fibers. One of the applications of this concept is found in the field of composite materials where the carbon fiber is embedded in epoxy or other polymeric matrix. The fibers, which traditionally serve as the main load resisting reinforcement, also serve as the sensory agents through monitoring changes to the electrical resistance of the fiber due to structural or ambient effects. The dual functionality of the fiber converts the composite structure into a self-sensory one with various sensing capabilities. Wen et al. (1999), Wang and Chung (1999b), and Guerrero et al. (2002) further developed this concept for temperature monitoring, whereas Wang and Chung (1996), Chung (2001b, 2007, 2012), Wang et al. (1998, 1999, 2006), Wang and Chung (1999a), Angelidis et al. (2004), Todoroki and Yoshida (2004), and Zhu and Chung (2007) adopted it for the detection of damage, strain, or fatigue.

Two other interesting applications of the aforementioned concept are directly relevant to RC structures. The first is found in the field of using carbon fiber-based composite bars as an alternative to traditional steel reinforcement (see, for example, Bakis et al., 2001; Nanni et al., 2009; Zdraveva et al., 2010). The second is found in the field of strengthening RC structures with externally bonded composite plates. In the latter, which also allows adding a sensory capability to an existing structural element, Mei and Chung (2000) and Chung (2001b) investigated the change in the electrical properties of the carbon fiber-reinforced polymer (CFRP) plate due to changes in temperature or debonding along the concrete-CFRP plate interface. Yang and Wu (2006) studied the ability of the CFRP plate to sense strain, propagation of cracks, and strain in the internal reinforcing steel bars.

Pioneering investigations of the characteristic of the electrical resistance in continuous carbon fibers embedded in cement-matrix composites, its correlation with the straining of the cement-carbon composite, and its potential use as a sensor have been conducted by Wang and Chung (1999a). Wen and Chung (1999) and Wen et al. (2000) first studied the concept of using continuous carbon fibers embedded in cement paste as

a sensory device. In Wen and Chung (1999) and Wen et al. (2000), the electrical resistance along the fiber direction was correlated to straining of the fiber due to uniaxial tensioning. In this layout, which is focused on a component level of a carbon fiber tow saturated with cement paste and tested under uniaxial tension, the tensile strain and therefore the changes to the electrical properties are equally distributed along the tow. The main observations reported in Wen and Chung (1999) and Wen et al. (2000) on the component level revealed that the electrical resistance increases upon tension in the tow's direction, and that the resistance change is mostly linear and reversible. These observations demonstrate the feasibility of using the continuous carbon fiber as strain sensors and support the step taken here from the single fiber or single tow scales to the structural TRC element scale.

The concept proposed in Wen and Chung (1999) and Wen et al. (2000) is reviewed in Chung (2000a, 2000b, 2001a, 2002, 2005), Wen and Chung (2007), and Xu and Chung (2001). These reviews highlight the sensing capabilities and also discuss the issue of installation costs. The concept proposed and examined in this study aims to move from the fundamental single tow scale (Wen and Chung, 1999; Wen et al., 2000) to the integrative TRC structural element scale and to augment the concept of sensing with continuous fibers to the structural scale. The focus of this article is on glass/carbon-based TRC structural element in which the same array of carbon tows contributes to the reinforcement required for the load resisting system and, at the same time, sets the basis for the sensory system and provides the structure with the self-sensory features. In the configuration outlined here, the carbon tows are embedded in a glass textile net, as part of the production of the textile, rendering its implementation in the concrete element a straightforward act. This aims to utilize the self-sensing capacity gained by means of the continuous carbon fibers and to significantly reduce or even eliminate the cost and labor inputs needed for converting the component into a sensory one. The shift from the single tow scale where the strain and the changes to the electrical resistance are uniformly distributed along the fiber (Wen and Chung, 1999; Wen et al., 2000) to the structural scale also exposes the monitoring system to local changes in the strain due to cracking of the concrete element under bending. These effects have not been addressed in the prior works that examined the single tow scale.

Along with aiming at the monitoring of strain, the article also aims at looking into the potential ability of the sensory textile to sense interaction with aqueous environment, wetting, and leakage. The effect of moisture on piezoresistivity of short carbon fiber-reinforced cement was investigated in Wen and Chung (2008). In this article, we aim to go beyond that and look at the response at the element level, examine the response of

continuous fibers that electrically links one side of the beam with the other, and look at the sensing of a localized and temporal wetting event. In that context, this study aims at further exploring the interaction with the aqueous medium and looks into scenarios where such interaction is triggered by penetration of water through cracks. This aspect is relevant to TRC systems that are directly exposed to such environments: pipelines for drinking water supply, wastewater systems, and so on. However, opposed to Wen and Chung (2008), which examined the coupled effect of strain and moisture, this article studies the effect of strain and the one of exposure to the wet environment separately.

Sensory textiles

The sensory textile combines two types of tows: tows made of glass fibers and tows made of carbon fibers. Optionally, it can also include embedded yarns made of stainless steel filaments (Berger et al., 2011; Goldfeld et al., 2014; Hegger et al., 2011; Quadflieg et al., 2013) or other materials, but these layouts are not at the focus of this work. The glass tows provide the main reinforcement platform. The carbon tows are also part of the main reinforcement and, at the same time, their electro-mechanical coupling of strain and electric resistivity (piezoresistivity) is used as the sensory agent. This feature designates the main advantage of the glass/carbon system. While metallic yarns embedded in the glass-based textile (Goldfeld et al., 2014; Quadflieg et al., 2013) also use the electro-mechanical features of the material for sensory capabilities, they do not contribute to the load-carrying capacity. The application of such metallic yarns is referenced here as an adjacent technology, whereas the focus in this work is on the hybrid sensory and structural carbon–glass textile.

A warp knitted grid structure with a mesh size of 7–8 mm is selected for the textile. The carbon tows and the reference stainless steel yarns (if present) have been inserted into the glass fiber grid in the warp knitting process as warp yarn. In the weft direction, glass fiber tows are used. The reinforcing yarns are then combined with warp-knitting yarns made of polypropylene. The stitch type of the warp knit is pillar. The production of the multi-material textile is illustrated in Figure 1. The production process is not involved with any modifications in terms of tribology or tension control of the fibers. This demonstrates the suitability of the selected fiber materials to be used in standard processes without any cost-intensive modifications.

The density of the glass fiber tows is 2400 tex and it is made of alkali resistant glass fibers. The properties of the glass tows are as follows: specific mass 2680 kg/m³, modulus of elasticity 72 GPa, and tensile strength 1700 MPa. The equivalent diameter (based on specific

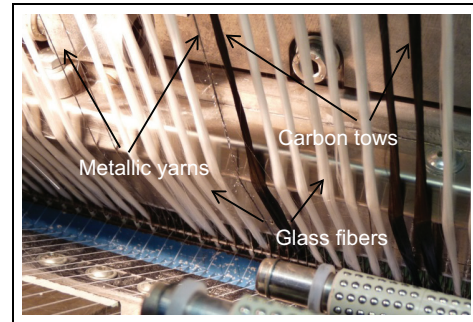


Figure 1. Yarns' and tows' insertion into warp knit.

weight consideration) equals 1.06 mm. The density of the carbon tows is 3300 tex with specific mass of 1800 kg/m³. Each tow comprises about 50,000 carbon fibers with filament diameter of 7 μ m. The elastic modulus of the carbon tows is 240 GPa and their tensile strength is 4000 MPa with elongation of 1.7%. Their electrical resistance per unit length equals 13 Ω /m. The metallic yarns are made of about 550 stainless steel 12 μ m filaments in two twisted yarns (275 filaments in each twisted yarn). The rupture load is 75 N at maximum strain of 10% and the electrical resistance per unit length is 14 Ω /m.

The setting of the textile in the molds, before and after casting, is illustrated in Figure 2. The electrical integration of the carbon fiber tows into the data acquisition (DAQ) system requires some attention. The process should assure effective physical, chemical, and electrical compatibility of the carbon tows with the overall electrical and mechanical systems. It should also provide a sufficient level of geometric stability, minimal impact on the electric circuit, and minimal parasitic electrical noise due to deformations in the connector. In the light of the above challenges, specialized techniques for the electrical linking of the sensory carbon fiber tow to the electrical system and the DAQ module are needed. Two layouts have been tested. The first one is based on a direct connection of the carbon tow to a conductive metallic wire using a conductive epoxy adhesive and rapid thermal curing. The end of the tow and the wire are bonded together using the conductive adhesive, the system is cured, and then covered and fastened together using a thermal shrinkable sleeve. In the second layout, a special mold has been developed for the fabrication of electrical connectors. The fabrication of this device is based on placing the carbon tow in the mold and then casting the connector using the conductive epoxy. The two layouts were examined with respect to the above criteria and it was found that although the first layout is very simple, it yields satisfactory results, mainly in terms of the geometrical stability of the connector, its sensitivity to deformations, and the resistance it incorporates into the electrical scheme. The simple connectors at the ends of each tow are shown in Figure 3.

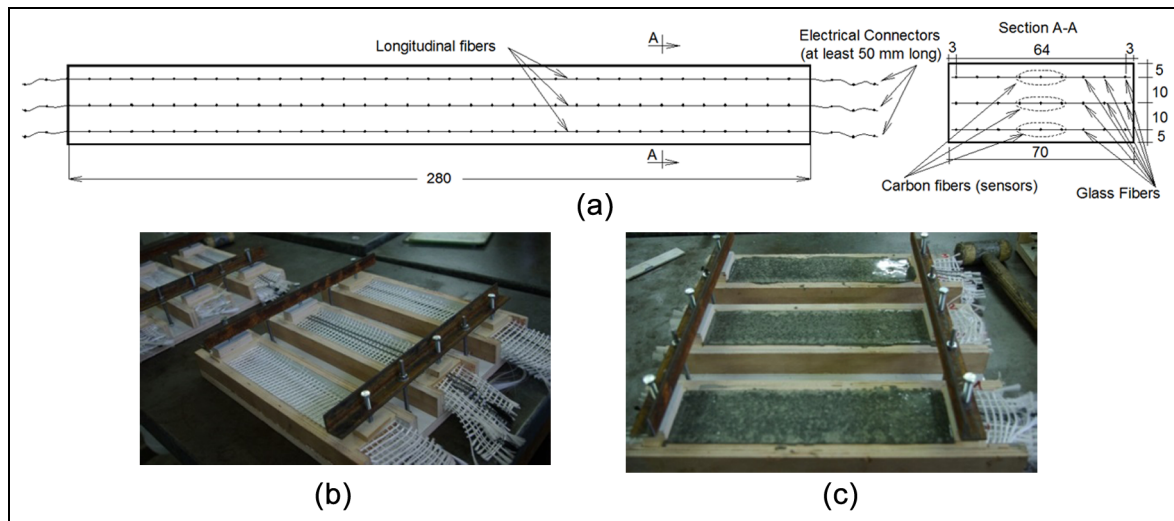


Figure 2. TRC specimens: (a) schematic drawing, cross section, and geometrical parameters (dimension in millimeters); (b) molds for three beams after placing the layers of sensory textile and before casting; and (c) molds after casting.

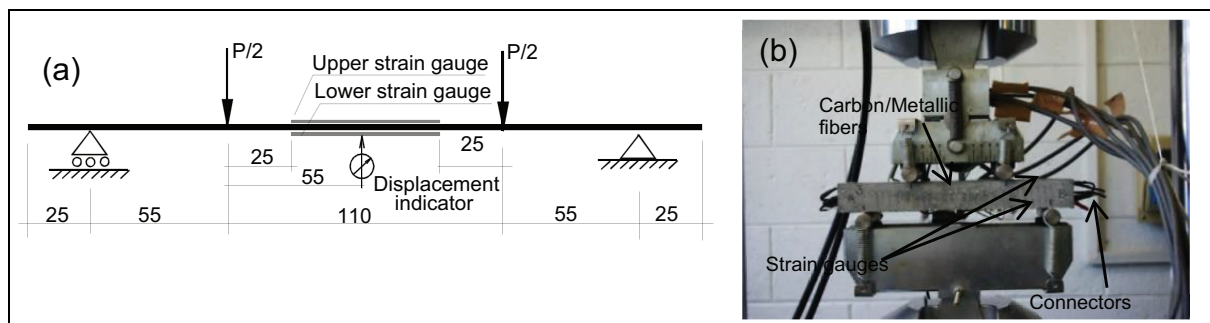


Figure 3. Four-point bending test of TRC beams: (a) loading scheme and “external” sensing (dimension in millimeters) and (b) the test specimen and the testing rig.

The TRC beam configuration studied in this work involves several carbon tows embedded in a single beam (see Figure 2). The structural action of the beam jointly utilizes all reinforcing tows but from the electrical point of view, each tow is connected to the DAQ separately and independently of the others. Other layouts including ones that reduce the numbers of channels and signals that has to be sampled simultaneously can be considered. However, this configuration has been adopted in order to compare the readings of adjacent tows as well as to look into the different responses of tows located at different levels along the height of the beam.

Design and production of TRC beam specimens

Four beam specimens reinforced with the sensory textile have been designed and casted. All specimens are 280 mm long, 70 wide, and 30–35 mm thick and they are reinforced with three layers of the smart sensory textiles. In the configuration studied here, the textiles are the only reinforcing component and the beams do

not include any additional metallic (steel bars) or other reinforcement. As a result, the structural and/or electrical interaction between the textile layers and such reinforcement is not studied here. Wen and Chung (2006) investigated this form of interaction in the case of short carbon fiber–reinforced cement paste. The design of a hybrid steel and textile-reinforced element similar to the ones studied here, the investigation of its sensory capabilities, and the assessment of the interaction between the textile and the metallic components are considered for further exploring this field.

The general layout of the beams, including the three layers of the textile reinforcement, is shown in Figure 2(a). Figure 2(a) also presents the cross section of the beam and the geometrical details of the three layers of textile reinforcement. One layer is located 5 mm above the bottom of the element, one is located 5 mm below the top of the element, and one layer is located at the middle of the beam. Pictures of some of the specimens before casting appear in Figure 2(b). Figure 2(b) also shows the molds developed in an attempt to maintain a preliminary low level of pre-tensioning, which has been performed manually, to all three layers of the sensory

Table 1. Properties of the grout (based on the manufacturer datasheet).

Density	2200 kg/m ³ (fresh mortar)		
Mechanical strengths (W/P = 0.13), at 25 °C	Compressive strength (ASTM C109)	1 day ~30 MPa	28 days ~65 MPa
	Flexural strength (BS4551)		~10 MPa
Elastic module (static)	~37,000 MPa		

smart textile and yet to allow penetration of the concrete mix. This is achieved using wooden spacers that are placed at the sides of the mold keeping the layers of textile at the desired height. The layers are manually tensioned and the wooden spacers are pressed against the mold using the steel bolts shown in Figure 2(b). The specimens after casting are shown in Figure 2(c). Each textile layer includes six longitudinal (0°) tows of glass fibers and two carbon tows. The transverse (90°) tows are all made of glass fibers. When a reference metallic yarn is used, it replaces a carbon tow.

The four specimens are divided into two groups that differ in the type of the longitudinal sensory tows. In the first group, each layer of sensory textile includes two longitudinal tows made of carbon fibers. These two specimens are designated CC1 and CC2. The second group includes one longitudinal carbon tow and one longitudinal metallic yarn per layer. These two specimens are designated CM1 and CM2. As mentioned before, the focus in this article is on the glass–carbon textile and its dual functionality as a structural component and a sensory agent. References to the glass–metallic specimens are brought here for the sake of comparison. A detailed discussion of the glass–metallic system appears in Goldfeld et al. (2014).

The beams are casted using a commercial grout mixture (Sika Grout 214). The mixture was prepared in accordance with the manufacturer instructions with 3.125 L of water per 25 kg of dry material (additional admixtures have not been used). The beams were cured in room temperature covered with a polymer sheet for at least 40 h. The properties of the grout, as reported by the manufacturer, are listed in Table 1. The tensile strength and the compressive strength of the grout were also determined using the procedure outlined in EN 196-1:2005 (2005). The tensile strength was determined through bending of 160 × 40 × 40 mm³ prisms (with measured dimensions that slightly differ from the ideal ones as listed in Table 1). After breaking, the beams in the flexure test, the compressive strength was evaluated by pressing the ~80 × 40 × 40 mm³ prisms through two 40 × 40 mm² steel plates. By means of this standard test, and in accordance with the test method, the dimensions listed in Table 1 refer to size of the compressing steel plates. The results of these standard tests, which were also conducted 40 h after casting, are listed in Table 2.

Table 2. Properties of the grout (based on testing according to CEN EN 196-1:2005, 2005).

Specimen No.	Dimensions (mm/mm)	Tensile strength (MPa)
1	41.3/160	6.83
2	41.2/160	8.20
3	41.1/160	7.75
Average ± STDV		7.59 ± 0.57
Specimen No.	Dimensions	Compression strength (MPa)
1	40/40	60.00
2	40/40	52.12
3	40/40	63.12
4	40/40	62.81
5	40/40	60.00
6	40/40	58.18
Average ± STDV		59.37 ± 3.66

STDV: standard deviation.

The experimental results reveal a good correlation with the data provided by the manufacturer.

Sensing concept

The fundamental physical phenomena upon which the monitoring capabilities of the TRC beams are based are derived from the changes to the electrical resistance of the carbon tows in the textile reinforcement. Here, a distinction is made between the sensing of strain, wetting, and accumulated damage. The detection of strain is based on the basic relationship between electric resistance and the ratio between the length of the resistor and its cross-sectional area. Straining of the tow under tension yields elongation and reduction in the cross-sectional area (although in the case of carbon fiber tows, the latter effect is probably less significant). Both effects increase the integrative electrical resistance of the tow. This phenomenon is well reflected by the experimental findings reported in the pioneering works of Wen and Chung (1999) and Wen et al. (2000) on carbon tows embedded in cement paste and subjected to a uniform tensile straining. Here, it is applied to the structural element level.

The shift from the fiber or tow scale and the uniform strains along the fiber tow (Wen and Chung, 1999; Wen et al., 2000) to the flexural element scale necessitates the consideration of strains that are not uniform along the

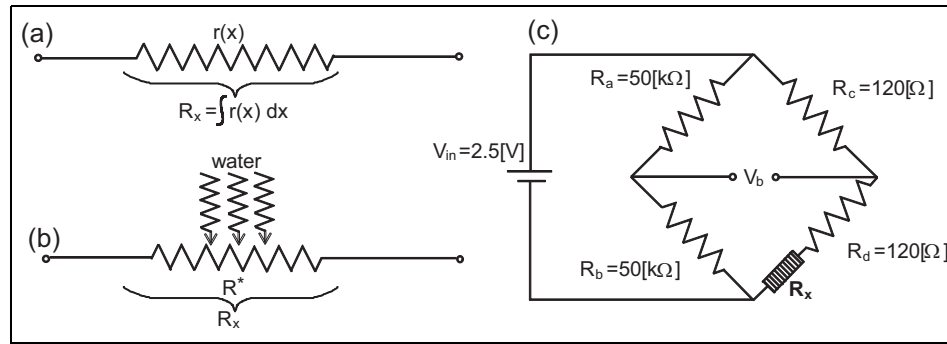


Figure 4. Electrical behavior of the carbon tow: (a) resistance layout due to straining, (b) resistance layout due to wetting, and (c) Wheatstone bridge (R_x designates the resistance of the carbon tow; V_b is the measured voltage).

tow. When the beam is subjected to bending, and especially when flexural cracks open, the distribution of strain is not uniform along the tow. However, since the resistance changes are measured from one end of the tow to another, the measured quantities are considered to be an integrative index. This means that only an integrative value of the resistance is evaluated. Such measure is illustrated in Figure 4(a) where $r(x)$ designates the resistance per unit length. $r(x)$ is affected by the straining along the tow and therefore changes along the tow. $R_x = \int r(x) dx$ integrates the effect of the distributed straining along the tow as well as localized ones in the close vicinity of cracks in the concrete.

The wetting of the carbon tow and the surrounding concrete body triggers several types of potential effects on the localized electrical scheme of the wetted region. First, the aqueous solution itself is conductive. Although the specific conductivity of the solution, which is based on ionic conductivity, is smaller than the electronic conductivity of the carbon fibers, it may still affect the localized properties of the wetted tow, as illustrated in Figure 4(b). A similar effect is discussed in detail in Wen and Chung (2008) who studied the effect of moisture on the piezoresistivity and the contact electrical resistivity of the fiber–matrix interface with fiber fraction below the percolation threshold. Above the percolation threshold, which characterizes the case studied in this article, the penetration of water into the capillary spaces in the tow may also affect the electrical interaction between the fibers it comprises. The localized analysis and quantification of the range of mechanisms that are triggered by the wetting necessitate a detailed micro-electro-mechanical investigation which can follow, for example, Wen and Chung (2008) but extend into the regime of continuous carbon fibers at the structural level. These aspects are not directly studied here, and this work only focuses on the global and integrative impact of the wetting. The micro-electro-mechanical investigation is designated as a subject for a future research work.

Damage in the form of cracking yields localized straining of the carbon tows bridging over the crack. If

the structure is exposed to a wet environment, cracking also allows the penetration of water through the crack and the wetting of the tow. Both effects impact the electrical resistance of the tow and allow the detection of such damage. This article studies the impact of each effect separately. The coupled effect looks at the straining of a beam in wet conditions (e.g. the study of Wen and Chung, 2008 on the piezoresistivity of carbon fiber–reinforced cement paste below the percolation threshold at the presence of moisture) or the wetting of a beam under load. Such coupled effects or the general coupling of straining and wetting at the structural TRC element level is also considered for future research in this field.

The common approach to measure the resistance change in a geometrically complex sample is the four-probe method. The four-probe method directly measures the resistivity of the specimen. It includes two outer probes and two inner ones. The electric current through the outer probes is controlled and the detection of the voltage through the inner probes allows measuring the resistivity of the examined body. The main advantage of the method is that it enables measuring the resistance in three-dimensional complex geometries, and that it is not influenced by the parasitic resistance of the auxiliary electrical setup (conductors, connectors). This method was extensively used for estimating the resistance change in short carbon fiber–based RC element (see, for example, Chen and Chung, 1993a, 1993b, 1995; Chung, 2000a, 2000b, 2003). However, the application of this method requires the installation of four probes, two of them within the element. In this study, we take advantage of the continuous configuration of the carbon tow and use a Wheatstone bridge setup to measure the voltage and the voltage change across the bridge in a two-probe mode. By means of the Wheatstone bridge layout and by using the known properties of all other resistors, the voltage change across the bridge can be converted to changes in resistance along the carbon fiber tow. In this method, only the two ends of the carbon tow are connected to the

DAQ and there is no need for additional external or internal connectors along the tow. This simplifies the installation of the tow in the concrete element and enables using this method for a spectrum of TRC structures without changing their structural geometry. The use of only two electrical contacts to measure the resistance can affect the measured initial value of the resistance due to the parasitic resistance of the auxiliary electrical components outside the tested specimen. This effect is mitigated here by means of the conductive epoxy connectors, the minimal external components of the circle, the assessment of the initial resistance values through the bridge setup, and the consideration of the relative change in the resistance with respect to the relative change in the strain.

The electrical scheme of the Wheatstone bridge and the specific properties of its resistors are presented in Figure 4(c). In this figure, R_x represents the resistance of the sensory tow (from one end to another). Following Kirchhoff's circuit laws, the voltage across the bridge, V_b , which is the quantity that is directly measured in this setup, is given by

$$V_b = \left[\frac{\rho_x}{R_c + \rho_x} - \vartheta \right] V_{in} \quad (1)$$

where

$$\rho_x = (R_d + R_x) \quad (2)$$

$$\vartheta = \frac{R_b}{R_a + R_b} \quad (3)$$

Consequently, the resistance of the tow R_x , which is the direct physical quantity that responds to straining or wetting, is given by

$$R_x = \frac{\vartheta R_c V_{in} + V_b R_c}{V_{in} - V_b - \vartheta V_{in}} - R_d \quad (4)$$

The properties of the known resistors in the bridge are $R_a = R_b = 50 \text{ k}\Omega$, and $R_c = R_d = 120 \text{ }\Omega$. The excitation voltage is $V_{in} = 2.5 \text{ V}$, the base value of V_b is about 20 mV , and the maximum change to V_b is $110 \text{ }\mu\text{V}$. This value corresponds to a resistance change of up to about $21 \text{ m}\Omega$. With this choice of properties, and since V_b is much smaller than V_{in} , the relationship between R_x and V_b is approximately linear. Based on the derivative of R_x in equation (4) with respect to the signal voltage V_b , the deviation of the relationship between ΔR_x and ΔV_b in the range of the changes detected by the electrical setup does not exceed 0.008% . In this study, we present both the voltage across the bridge, which is the quantity that is directly measured, and the resistance change, which is the actual physical quantity that is affected by the straining and/or wetting.

The concept adopted here for the self-sensory TRC element uses a macroscopic approach and detects the integrative effect of strain, damage, or wetting on the

sensory tow. Physical effects that take place on a more localized scale, including the extent of the penetration of grout into the tows, probably affect the mechanism of the sensing. The above effect as well as other micro-mechanical features of the embedded tow is measured and considered as a part of the macroscopic characteristics. Exploring the range of micro-mechanical features of the embedded tow and its interaction with the cement matrix on the microscopic level is designated for future research in this field.

Sensory TRC elements—experimental validation

Mechanical and electrical test setup

The mechanical testing of the beams was conducted using an MTS machine in a displacement control mode. The beams were tested in a four-point bending scheme as illustrated in Figure 3. All tests were conducted under a uniform loading rate of 0.25 mm/min . Along with the internal sensory textile, the test included monitoring of the load, the crosshead location, the vertical displacement at the middle of the beam, and the strains at the upper and lower faces of the beams. The external strains were measured by two 60-mm -long strain gauges mounted on the upper and the lower faces.

Structural response of the TRC beams

This section examines the response of the TRC beam to mechanical load and characterizes its structural behavior. The ability of the carbon tows to “sense” the process is examined and quantified in the following sections.

Figure 5 depicts the load versus deflection curve for beam CC1 and the readings of the two surface mounted (external) strain gauges. The strains measured at the outer faces of the beam and the assumption of a linear strain distribution allow assessing the variation in the strains through the thickness of the beam

$$\varepsilon(z) = \frac{\varepsilon_b + \varepsilon_t}{2} + \frac{\varepsilon_b - \varepsilon_t}{H} z \quad (5)$$

where $\varepsilon(z)$ is the distribution of strains; ε_t and ε_b are the strains at the upper and lower faces of the tested beam measured by the strain gauges, respectively; H is the height (thickness) of the beam; and z is the vertical coordinate, which is measured from the middle of the beam downward. Pictures of the tested beam at different stages of the loading process appear in Figure 6.

The load–deflection curve and the strain–deflection curves (Figure 5) reveal four main phases that characterize the structural response of the TRC beam. The first phase is the initial response of the un-cracked beam. Note that the measurements are recorded from the very first contact of the loading machine and the

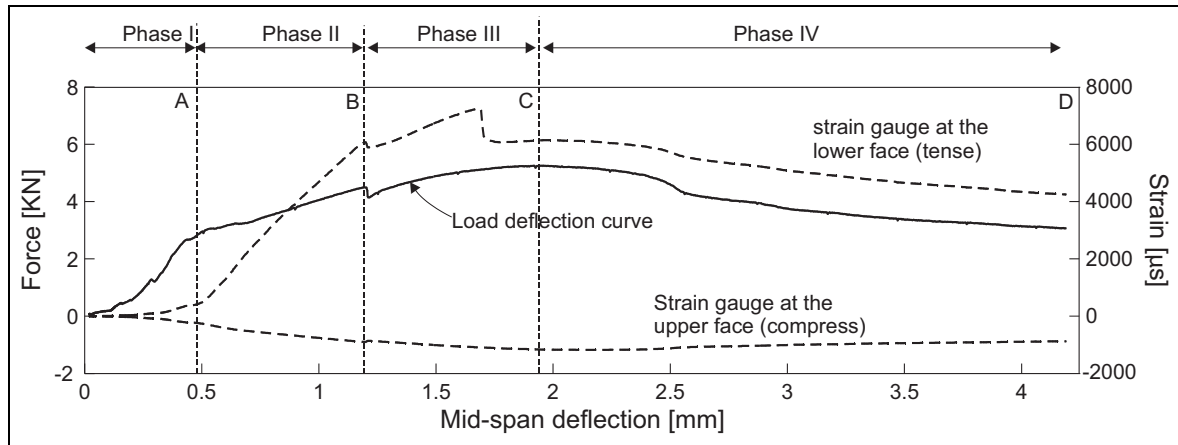


Figure 5. Structural response of beam CCI: load versus deflection and strain measured by external strain gauges versus deflection.

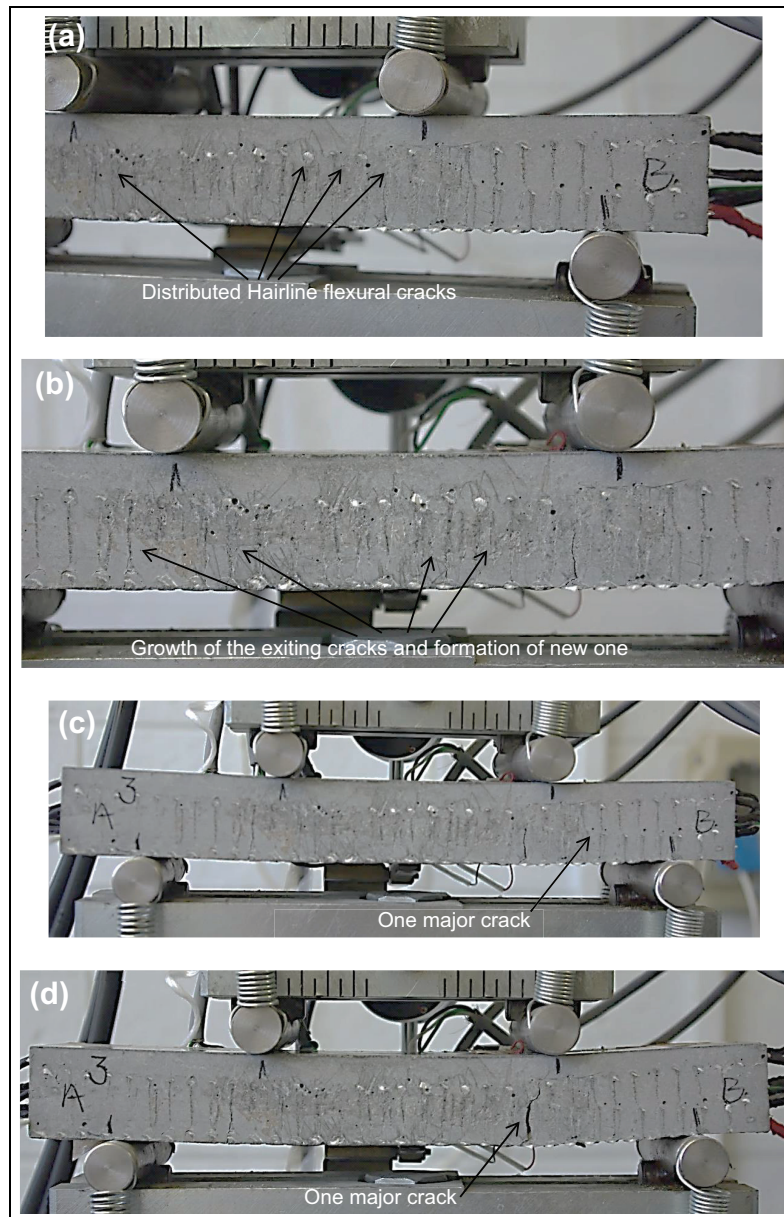


Figure 6. Beam CCI at different stages of the loading process (a) phase I, (b) phase II, (c)-(d) phase III.

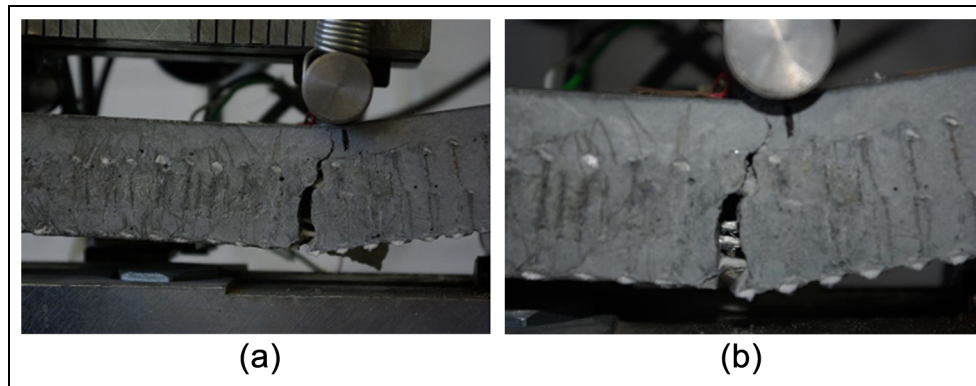


Figure 7. Major crack at beam CCI at the end of the test: (a) side view and (b) zoom on the crack.

beam; therefore, the initial steps are attributed to the settlement and the slight self-organization of the test setup. After that, this phase reveals an almost linear response up to a load level of about 2.75 kN (point A) where the first flexural cracks are visually detected. The development of cracks from this point and on is well reflected by the change to the slope of the load–deflection curve and by the change to the strain evolution curves at point A.

The second phase of the response starts after the initiation of cracking at point A. As expected, the formation of flexural hairline cracks (detected by visual inspection, see Figure 6(a)) yields a reduction in the stiffness of the beam manifested in the slope of the load–deflection curve and in the increase in the rate of growth of the strains. The flexural cracking and the resistance of the global bending moment by means of compression in the concrete and tension in the reinforcing textile also shift the height of the neutral axis of zero longitudinal strain upward. As a result, the tensile strains at the lower face grow much faster than the compressive ones at the upper face. This effect, which is clearly observed in Figure 5, reflects a typical behavior of a TRC flexural member.

The cracking pattern detected in the second phase of the response includes a series of distributed hairline flexural cracks. These cracks did not propagate evenly through the beam width. Some opened at the front side of the beam and propagated to the back and others propagated from the back to the front. A further monotonic increase in load, deflections, and curvatures leads to the growth of the existing cracks as well as to the formation of new ones, see Figure 6(b). The opening of additional hairline cracks and their distribution (opposed to the development of one large crack) reflects good anchorage of the textile in the matrix, effective bond of the textile and the concrete, and minimal slip between the two. It also reflects a favorable behavior in terms of structural response at the post-cracking stage where the ability of the element to resist bending moments critically depends on the reinforcing textile. Finally, the

evolution of many distributed hairline cracks reflects a favorable structural behavior in terms of durability.

The third phase of the structural response starts at a load level of about 4.5 kN (point B in Figure 5). At this point, the load slightly drops and one major crack starts to develop very close to the right loading point. The opening of this single crack is well observed in Figure 6(c) and (d) and it is accompanied by a gradual reduction in the slope of the load–deflection curve up to the peak load (point C). Then, in the fourth phase, a monotonic reduction in load is observed up to the point where the test has been terminated (point D). To avoid damage to the setup, the test has been terminated before total failure or collapse. Similar trends are observed in the response in terms of the tensile strains at the lower face of the beam (Figure 5). These observations are also typical to flexural RC elements at the final stages of their loading process where failure mechanisms take over.

During the final stages of the response and along the evolution of the failure mechanism, the reinforcing textile kept bridging the opening cracks. This effect is demonstrated in Figure 7(a) and (b), which shows a zoom plot on the opened crack. Rupture or pull out of the longitudinal reinforcing tows or rapid drops in the load were not observed. Rapid drops in the load at the final loading stages, rupture of the textile, or pull out of the tows were not observed in the other tested beam as well. These observations clarify that the textile reinforcement provides the structural element with the ability to maintain its integrity at failure without a sudden release of load. Opposed to the elasto-plastic behavior of the steel reinforcement traditionally used in RC elements, the reinforcing glass and carbon fiber–based textile layers are basically linear and elastic. Therefore, the beam does not reveal a significant level of plasticity and displacement ductility. Yet, the results clearly reveal a sound ultimate state response that is not involved with an abrupt failure or a sudden loss of structural functionality. This demonstrates the structural capabilities of the TRC element.

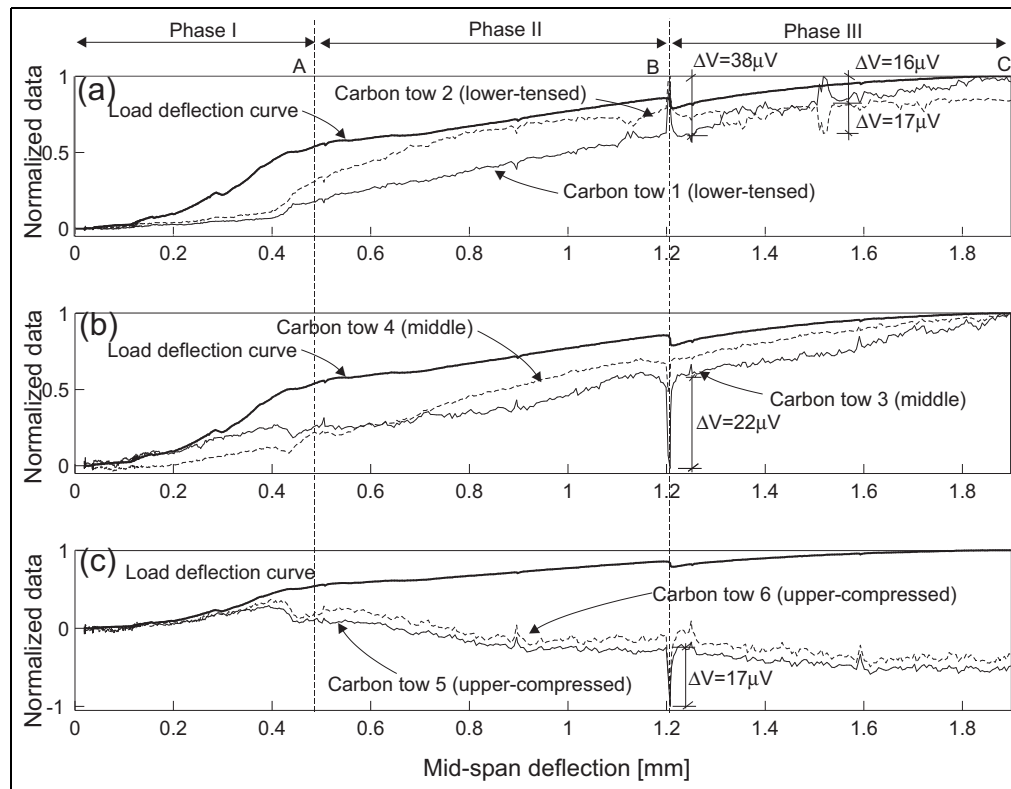


Figure 8. Normalized electrical readings of the carbon tows in beam CCI and normalized applied load versus mid-span deflection: (a) lower carbon tows, (b) middle carbon tows, and (c) upper carbon tows.

The concept adopted here for the structural assessment and examination of the TRC element uses a macroscopic approach with respect to its structural response. Physical effects that take place on a more localized scale, including the extent of the penetration of grout into the tows, probably affect the structural mechanism. As for the latter, the visual inspection of the cross sections after cutting the tested beam into pieces as well as visual inspection of the opened cracks (Figure 7(b)) did not reveal significant penetration of cement paste into the spaces within the carbon tows. With the focus on the macroscopic (element level) structural response, the above effect as well as other micro-mechanical features of the embedded tow are accounted for as a part of the macroscopic characteristics. Breaking the macroscopic behavior into more localized mechanisms, exploring the range of micro-mechanical features of the embedded tow, and characterizing its interaction with the cementitious matrix on the microscopic level (e.g. Wen and Chung, 1999, 2008) are designated for further research in this field.

Strain sensing

The first step in the examination, characterization, and potential demonstration of the sensing capabilities of the TRC element is the investigation of the electrical

reading of the carbon tows. Since the physical index that is actually measured is the voltage across the bridge, the investigation first focuses on the measured voltage, which is presented in a normalized form. In parallel, the electrical resistance, which is the physical parameter that directly responds to the straining, is quantitatively examined. The normalized voltage readings for the carbon tows in beam CCI are plotted and qualitatively compared with the normalized load–deflection curve in Figure 8. The quantitative resistance changes are studied in Figure 9. The results shown in Figure 8 refer to voltage and they are normalized using the peak value. The load–deflection curve is also normalized and plotted in a scaled form on the same range of 0–1. The highest voltage change in each tow is specified in the figure. This normalized representation allows to study the qualitative correlation between the electrical readings of the carbon tow and the mechanical behavior of the beam, as reflected by the load–deflection curve. The resistance changes for each tow, calculated by equation (4), compared with the load–deflection curves, are presented in Figure 9. This figure, which quantitatively shows the changes to the physical parameter that is directly affected by the mechanical response, also includes the relevant information regarding the initial resistance values of each tow. Comparing those values to the theoretical ones stemming from the

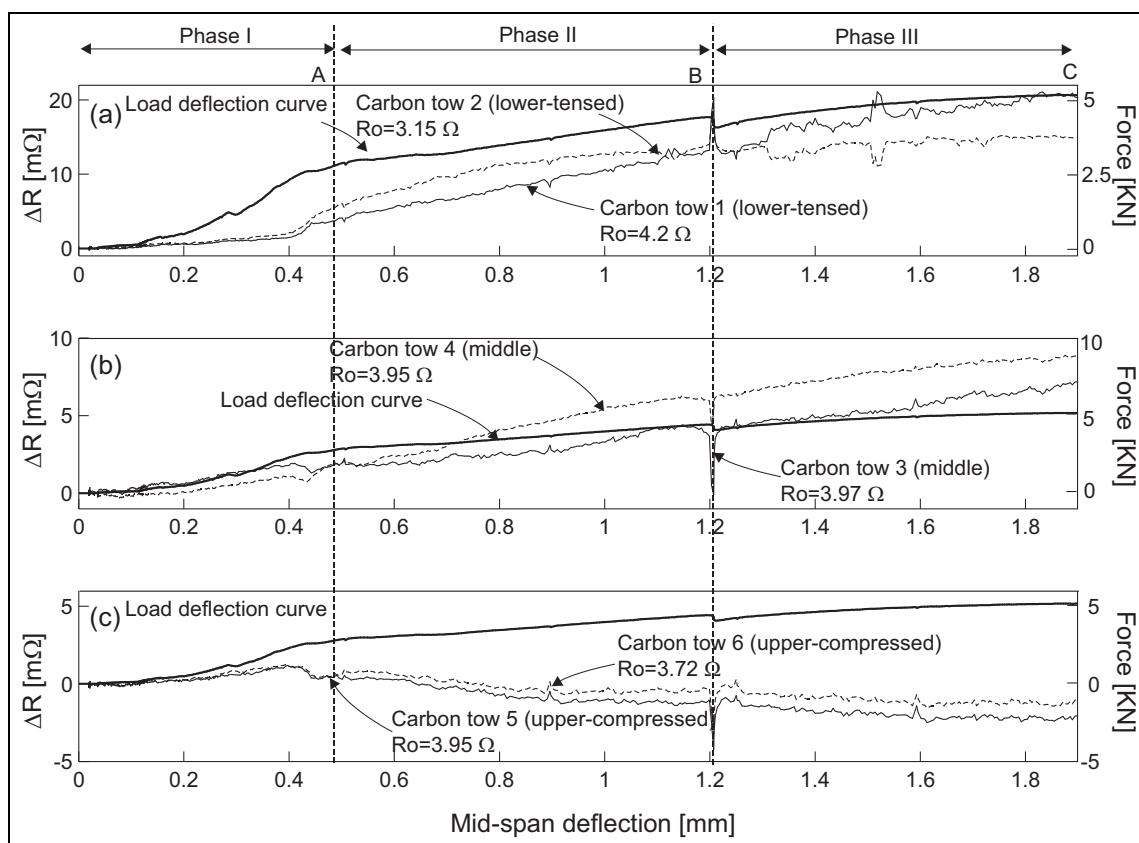


Figure 9. Resistance changes in the carbon tows in beam CC1 and the applied load versus mid-span deflection: (a) lower carbon tows, (b) middle carbon tows, and (c) upper carbon tows.

resistance per unit length of the carbon tows, it appears that the impact of the connectors on the initial value is not too significant, and that the measured values do not change much from one tow to another. To complete the quantitative representation of Figure 9, the quantitative correlation between the voltage, the resistance change, and the detected strain is studied later in this section.

For simplicity, the presentation of the normalized electrical readings (Figure 8) and the resistance changes (Figure 9) is divided into three separate figures. Figures 8(a) and 9(a) refer to the two carbon tows near the lower face of beam CC1. Figures 8(b) and 9(b) refer to the two carbon tows near the middle of the same beam. Figures 8(c) and 9(c) refer to the two tows near the upper face of that beam. The following discussion is limited to the ascending loading branch (up to point C). The post-peak descending branch is then discussed at the end of section “Calibration.”

The trend of the electrical readings (voltage, resistance) and their qualitative comparison with the trend of the load–deflection curves reveal that the sensory tows provide sound and relevant information about the flexural behavior of the tested beam. Figures 8(a) and 9(a) show that the readings of the two lower carbon tows are affected by the initiation of cracking at point

A. This event is well reflected by the change to the slope of the normalized voltage and particularly by the faster growth of the changes to the electrical resistance. A similar change in trend is also observed in the electrical readings of the two sensory tows located near the upper face (Figures 8(c) and 9(c)). Yet, on the quantitative scale, the changes to the resistance (Figure 9) are about four times smaller than the ones observed in the lower tows. Figures 8(b) and 9(b) show that the readings of the tows located near the middle of the beam are not so sensitive to the formation of distributed hairline cracks. In these tows, which are located near the original (pre-cracked) neutral axis, the changes to the structural behavior at point A are not well reflected.

The behavior of the sensors at point B, where the significant flexural crack opens, is slightly different, and also here the layers of sensory textile well reflect the structural event. At point B, all six carbon tows reveal a significant but temporary peak in their electrical readings (voltage and resistance). The formation of this temporary peak is in agreement with the drop in the load observed in the load–deflection curve. This means that the electrical readings of the reinforcing textile well reflect the significant event in the structural response of the TRC beam. On the quantitative scale (Figure 9), it appears that the temporal perturbation at

point B is detected by all carbon tows with a similar magnitude of resistance change. This reveals the impact of the cracking at point B, the structural effect it triggers, and the potential ability to have it detected by the monitoring system, regardless of its location through the height. This observation is particularly relevant to structural schemes where the bending moment diagram changes its sign along the beam and the tensioned side shifts from one face of the beam to another.

In all three pairs of carbon tows, the electrical reading of one tow is very close to the reading of the other. This is clearly observed in spite of the presence of the noise of the electrical data, which has not been smoothed or canceled out. The correlation is observed qualitatively in Figure 8 and, more important, quantitatively in Figure 9. In spite of the slight differences in the initial, reference resistance from one integrated tow to another, which are mainly attributed to the use of the two-probe mode by the Wheatstone bridge configuration and the associated impact of the parasitic resistance of the connectors, the readings of each pair of neighboring tows are very close one to another. This clarifies that in spite of the drawbacks of the two-probe mode (compared with the four-probe one), here it provides reasonably reliable and consistent readings.

Calibration

The calibration of the sensory textile is conducted by matching the electrical readings of each carbon tow with the strain readings detected by the strain gauges and interpolated to yield the strain at the level of the tow (equation (5)). In equation (5), the strains at the top and the bottom of the beam are estimated by the strain gauges mounted on the upper and lower faces, respectively. The heights of the layers (z) have slightly shifted during the casting of the beams and the strain interpolation is based on the actual heights measured after cutting the tested beams. By means of these parameters, the estimated strain at the textile level (height) is evaluated.

The calibration procedure can be performed by correlating the voltage change (the measured value) and the estimated strain. The outcome of this procedure can be used for directly estimating the structural response. Alternatively, calibration can be performed by correlating the relative resistance change and the

strain. This can be used in order to further define a gauge factor. Both types of calibration are presented next.

The link between the measured voltage change and the strain is first calibrated through a linear relation. The calibration process and the quantitative consideration of the electrical readings also include aspect of the quality of the signal and the signal-to-noise ratio (SNR). Therefore, the process is applied to the measured voltage change, which is the physical quantity that is directly measured in the test. The quantitative consideration of the changes to the resistance and the corresponding gauge factor are considered in the second part of this section. The linear voltage change to strain scaling factor, $C_{\Delta V 2 \varepsilon}$, is determined by minimizing the error given by the following expression

$$err = \left\| \varepsilon(z_{Tow}) - C_{\Delta V 2 \varepsilon} \cdot \frac{\Delta V_b}{V_{in}} \right\|_2 \quad (6)$$

where err is the error to be minimized, $\varepsilon(z_{Tow})$ is the interpolated strains at the level of the examined tow (z_{Tow}) evaluated by equation (5), ΔV_b is the electrical reading (voltage change) of the relevant tow, V_{in} is the excitation voltage (2.5 V in this case), $C_{\Delta V 2 \varepsilon}$ is the factor to be determined, and $\|\cdot\|_2$ is the L_2 -norm.

This calibration process is limited to the initial ascending branch of the response up to the first significant change in the structural behavior. It does not include the evolution and opening of the significant crack near the loading point. An alternative calibration scheme could be limited to the initial linear phase of the response where cracking and other nonlinearities do not come into effect. However, preliminary numerical experiments have shown that limiting the calibration to this initial phase does not yield satisfactory results. This is mainly attributed to the resolution of the signals under the relatively low levels of strains. To avoid this limitation, the calibration is extended to the entire ascending branch of the response up to point C.

The results of this calibration process appear in Tables 3 and 4. These tables also list information that reflects the quality of the electrical signal detected by the tows. This information includes the root-mean-squared (RMS) amplitude of the electrical signal for each tow, the RMS amplitude of the electrical noise, and the SNR in each sensor. Based on the results that

Table 3. Linear calibration factors for beam CC1.

Tow No.	Fibers	Location	Height (mm)	Signal RMS (μ V)	Noise RMS (μ V)	SNR (dB)	Calibration factor
1	Carbon	Bottom (tensed)	7.50	41.13	0.98	32.45	100
2	Carbon	Bottom (tensed)	7.50	43.07	1.11	31.77	127.5
3	Carbon	Middle	-2.50	13.27	0.60	26.89	182.5
4	Carbon	Middle	-1.50	19.31	0.71	28.69	137.5
5	Carbon	Top (compressed)	-14.0	4.64	1.14	12.19	-52.5
6	Carbon	Top (compressed)	-14.0	2.94	0.65	13.10	42.5

RMS: root mean square; SNR: signal-to-noise ratio.

Table 4. Linear calibration factors for beam CM1.

Tow No.	Fibers	Location	Height (mm)	Signal RMS (μV)	Noise RMS (μV)	SNR (dB)	Calibration factor
1	Carbon	Bottom (tensed)	15.0	69.38	0.40	44.78	72.5
2	Metallic	Bottom (tensed)	15.0	405.00	1.57	48.23	-11.5
3	Carbon	Middle	6.0	9.30	1.10	18.54	410
4	Metallic	Middle	6.8	87.50	0.60	43.27	-27.5
5	Carbon	Top (compressed)	-10.0	31.12	0.78	32.02	32.5
6	Metallic	Top (compressed)	-10.0	27.69	0.64	32.72	-31

RMS: root mean square; SNR: signal-to-noise ratio.

are summarized in Tables 3 and 4, the following observations are made:

1. The carbon tows located at the tensed face of the beam reveal a stable sensory behavior with stable calibration factors and acceptable SNR. This observation further supports the use of the electrical readings of these tows as a basis for the sensory system.
2. There is a significant difference between the calibration factors attributed to sensors located at the lower face of the beam and sensors located at the middle and upper face of the beam. ANalysis of VArance (ANoVA) test of the top, middle, and bottom calibration factors shows a statistically significant difference between groups as determined by one-way ANoVA ($F_{(2,6)} = 6.489349$, $p_{value} = 0.031598$). In beam CC1, the calibration factors for the tows at the bottom and the ones at the middle are similar, but the ones for the tows at the top significantly differ. The results detected in beam CM1, which combines carbon tows and reference metallic yarns, reflect trends that are not as clear as the ones observed in beam CC1. Yet, it still reveals notable differences between the upper and the lower groups.

The differences between the upper and the lower measurements are also reflected by the quality of the electrical signal. This is well observed in the RMS measure of the signal and mainly by the SNR. The SNR indexes attributed to the sensors at the bottom of the beams are much higher than the ones attributed to the sensors at the middle and the top of the beams. Excluding metallic yarn No. 4 in beam CM1, this observation is relevant to all other 11 tows and yarns.

The above observations are attributed to the different physical behaviors of the three groups of tows. The lower tows are subjected to tensile forces that are significantly amplified due to cracking of the beam. The tows in the middle are close to the neutral axis and, at least at the initial stages of the response, they are not

subjected to a significant level of strain. The sensory tows at the upper face are subjected to compression. Based on the structure of the tow and the fibers that it is made of, its ability to resist compression and to translate the compression into effective electrical readings is not expected to be significant. This is well reflected by the reduced electrical amplitudes of the signal detected by the neutral or compressed tows. As a result, the calibration factors attributed to the compressed tows are less consistent (see, for example, beam CC1). In fact, since the reinforcement is effective in tension, these results and the above discussion imply that the use of the sensory feature of the textile should be limited to tension only. Compressive readings should be disregarded.

3. The tensioned carbon tows reveal reasonable consistency and a reasonable repeatability of the calibration factors. Specifically, calibration factors detected for the two lower carbon tows in beam CC1 (Table 3) and for the lower carbon tow in beam CM1 (Table 4) are in reasonable agreement. This level of consistency is not observed in the compressed carbon tows where Table 3 (beam CC1) reveals a good agreement but Table 4 (beam CM1) reveals a sign reversal. These observations strengthen the one discussed in Item 2 and imply that the use of the carbon tows as sensors should be limited to the tensioned reinforcement.
4. The readings of the metallic yarns, which follow the steps discussed in Quadflieg et al. (2013) and Goldfeld et al. (2014) and brought here for the sake of comparison, are less consistent than the ones of the carbon tows. This is relevant to the tensioned metallic yarns, which reveal a reversal of the sign in beam CM1. The tensed carbon tows do not reveal such reversal of sign but provide relatively consistent values.

The next calibration step correlates the electrical readings in terms of electric resistance change with strain.

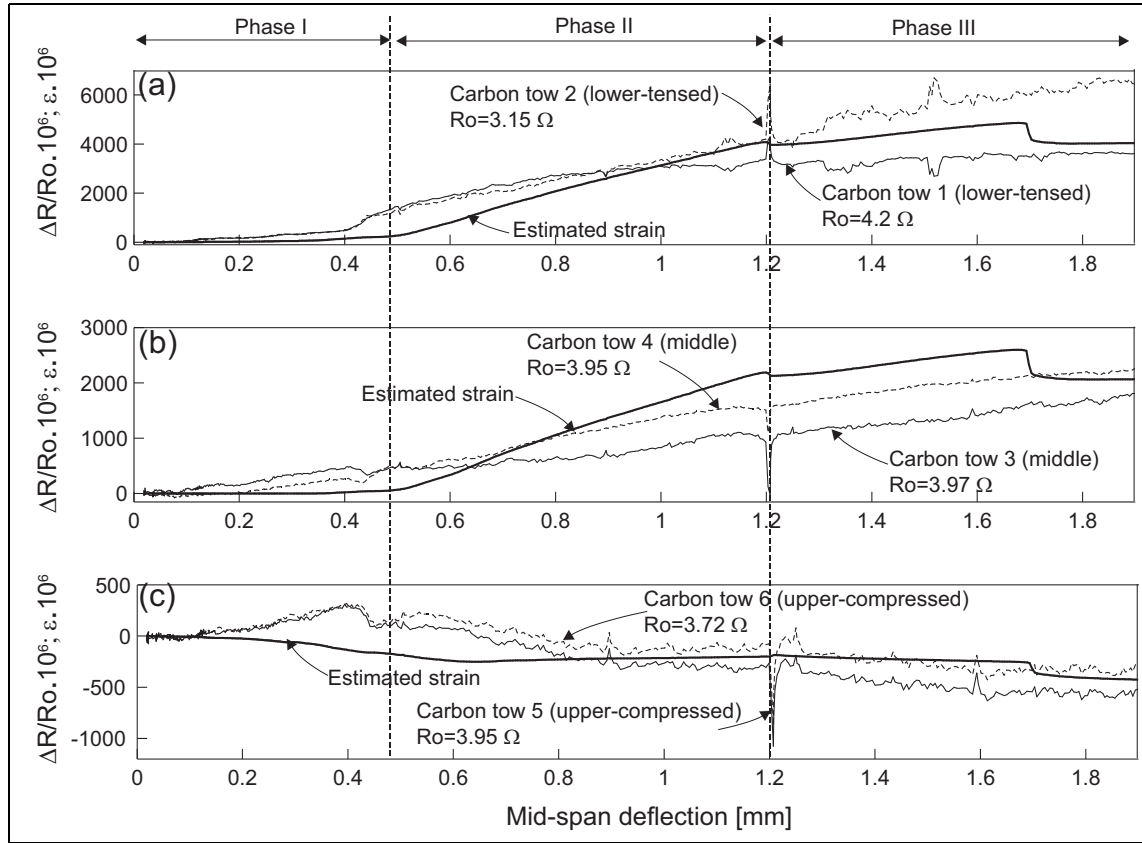


Figure 10. Relative resistance change and estimated strain of the carbon tows in beam CCI versus mid-span deflection: (a) lower carbon tows, (b) middle carbon tows, and (c) upper carbon tows.

This procedure aims to estimate the integrated gauge factor of the electro-mechanical sensory system. The gauge factor is defined as the relative change in the resistance per unit strain

$$GF = \frac{\Delta R/R_o}{\epsilon} \quad (7)$$

where R_o is the initial resistance, ΔR is the resistance change due to straining, and ϵ is the strain. In this study, the electric resistance is calculated by equation (4) and the strain by equation (5). Figure 10 depicts the relative change in the resistance ($\Delta R/R_o$) with respect to the estimated strain at the tow's location versus the displacements. The strains are estimated in the middle of the beam ($x = L/2$) based on the strain readings which are averaged along the relatively long (60 mm) external strain gauges. The relative change in the resistance refers to the integrative value along the tow. The two quantities are examined for all six carbon tows in beam CCI and along the first three phases of the test. According to Figure 10 and mainly based on the comparison between the results in terms of strain and those in terms of fractional resistance change, it is observed that a gauge factor of the sensory system is of the order of 1. Wen and Chung (1999) and Wen et al. (2000) found that for a continuous carbon fiber tow embedded in a cement paste

and subjected to uniaxial tension, the gauge factors range from about 17 up to 60 with a slight dependency on the loading cycle and the fiber volume fraction. The lower values that are detected in this study are attributed to the less "sterile" sensing environment associated with the flexural element, the variation in strains along the beam, the localization of resistance changes due to cracking, and the extension of the test throughout the entire non-linear response of the structural element.

The observations discussed above support the idea that the glass/carbon fiber textile can be used as reinforcement and a sensory device at the same time. This study focuses on investigating the ability of the textile to macroscopically sense structural response in a concrete structural element. However, in order to bring this concept to be fully realized, further investigation is still needed. Among the variety of aspects that still have to be looked at, the quantification of the reversible and irreversible components of the resistance changes in RC element is an important one. Wen and Chung (1999) and Wen et al. (2000) studied this phenomenon and demonstrated the reversibility of the electrical readings for uniaxial continuous carbon tow embedded in cement paste. Based on their observations, the extension of the scope into the field of cyclic response and the characterization of the reversibility of the response at the flexural element scale are designated as directions for future research.

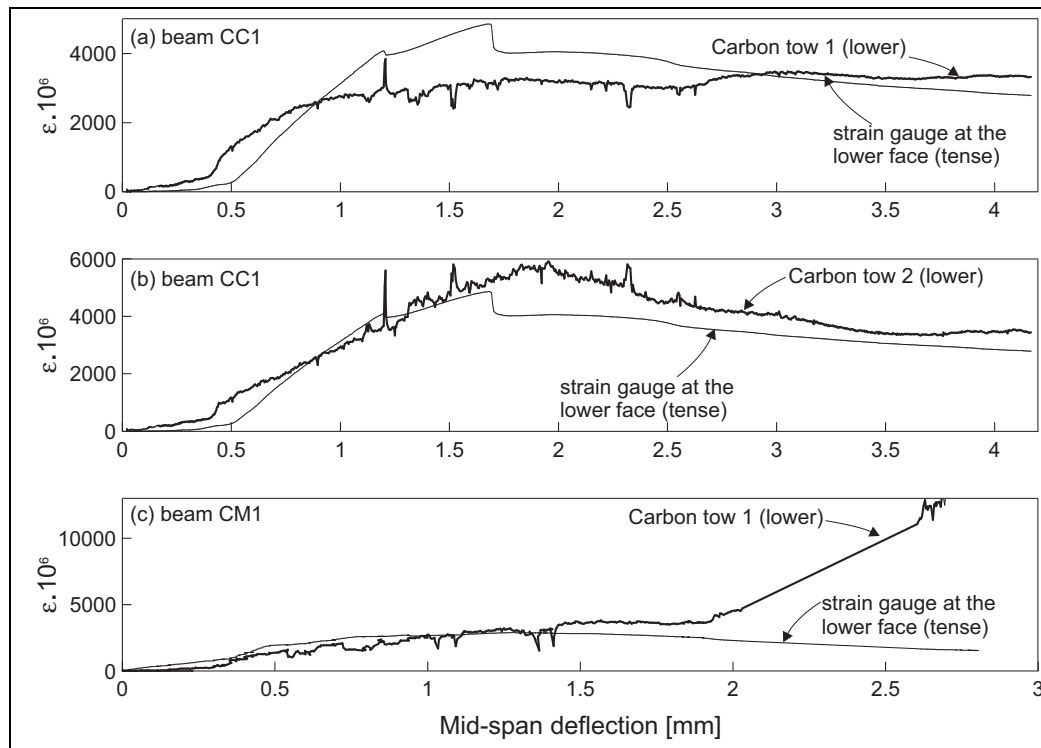


Figure 11. Strain reading of the sensory carbon tows compared with strains interpolated using the readings of the strain gauges: (a) tow No. 1 in beam CC1, (b) tow No. 2 in beam CC1, and (c) tow No. 1 in beam CM1.

In order to summarize the examination of the quantitative strain sensing capabilities, the behavior of the sensory carbon tows throughout the entire loading process is examined. Based on the observations and findings discussed earlier in this article, the examination focuses on the tensioned carbon tows. This includes tows 1 and 2 in beam CC1 and tow 1 in beam CM1. In Figure 11, the calibrated readings of the tensioned carbon tows are compared with the strains interpolated using the readings of the external strain gauges. This comparison, which extends through the entire loading range, also considers changes to the height of the neutral axis due to cracking of the concrete beam.

Figure 11 reveals that the sensory textile provides a reasonable assessment of the strains in the TRC beam. This is particularly observed in tow 2 in beam CC1. The agreement extends even beyond the peak load and beyond the range that was used for calibration. The quality of the assessment slightly changes from one beam to another and from one tow to another. However, in all cases, the major events in the structural behavior of the beam and the magnitudes of strains are reasonably captured.

Sensory response to wetting

The last part of the experimental study examines a completely different sensory capability of the smart reinforcing textile. This part focuses on the electrical response

of the carbon TRC specimens to wetting. The importance of the detection of wetting is dual. First, it aims to detect the functionality of the TRC member in terms of exposure to water or even potential leakage in water supply systems or wastewater pipelines. This feature is critical for avoiding loss of drinking water or mitigating the hazard of environmental pollution. Second, by means of the interaction with the aqueous environment, it aims to gain more information on the structural state of the element and to detect damage in the form of cracks.

The evolution of hairline cracks in the TRC system at the initial stages of the nonlinear response and the significant crack opening at the progressive loading stages expose the textile reinforcement to the environment. Therefore, the hypothesis is that this type of cracking and the exposure of the sensory textile to a conductive aqueous solution provides detectable electrical readings. Such readings can serve as a basis for the functional monitoring. It should be noted that the current investigation makes a distinction between the sensing of strain and the sensing of wetting. In the mechanical tests described in the previous section, the beams were not exposed to wetting. In the wetting test described next, the tested beam is not mechanically loaded and the electrical response is only due to wetting. The coupled effect was studied by Wen and Chung (2008) in the context of the impact of moisture on the piezoresistivity of cement paste reinforced with

short carbon fibers but with fractional fiber content below the percolation threshold. In the present case, the sensing and the wetting events in flexural elements reinforced with continuous carbon tows (which form an electrical conductivity mechanism above the percolation threshold) are studied, but the coupled effect of sensing strain and wetting at the same time is considered for future study.

In order to present reference observations on the response of a single isolated carbon tow to wetting, the influence of water on the electrical resistivity of the carbon tow is studied first. The hypothesis claims that the wetting of the tow and the penetration of water into the capillary spaces in the carbon tow yield a localized change in the electrical resistance, which transform into a measurable change in the integrative resistance of the entire tow; see Figure 4(b). The micro-mechanisms that derive these changes may vary from the effect of the ionic conductivity of the solution to micro-changes to the structure of the tow and their influence on the interaction between the fibers it comprises. The investigation of these micro-mechanisms, which may amplify or cancel out each other, is beyond the scope of this article, which only focuses on the macroscopic observations.

A single carbon tow, slightly tensed in the open air is wetted using two types of aqueous solutions. The first one is distilled water with a measured conductivity of $1 \mu\text{S}/\text{cm}$ and the second one is tap water with a measured conductivity of $1200 \mu\text{S}/\text{cm}$. During the test, different points along the tow were subjected to localized wetting. In each wetting event, a $20 \mu\text{L}$ drop of water is placed on the tow. This quantity wets a limited region of about 5 mm. The tow itself is hooked to the same Wheatstone bridge layout presented in Figure 4(c). The continuous changes to the resistance of the tow are outlined in Figure 12. The initial resistance values are depicted in the figure. It is clearly seen that the wetting events are well detected by the monitoring system in the form of a jump in the resistance. Furthermore, it is observed that the conductivity of the water directly

affects the level of change to the resistivity of the entire carbon tow. While both aqueous solutions have the same impact on temperature, which also affects the integrative electrical resistance, the changes observed with the tap water are about two to three times larger than the ones observed with the distilled water.

The second phase in exploring the detection of wetting focuses on the TRC flexural element level. The electrical response of the carbon-based TRC beam specimens to wetting is examined in Figures 13 and 14. The discussion focuses on the response of all carbon tows in beams CC1 and CC2. The initial values, R_o , are presented in the relevant figures. The electrical setup and the integration of the carbon tows into the DAQ are identical to the ones used in the mechanical testing phase. At this stage, the study of the response to wetting is limited to the electrical readings in terms of resistance changes. Linking these quantitative values to the structural or functional state of the beam (distribution of cracks, location and/or width of cracks, the rate of water percolation, etc.) is considered for further investigation.

Figure 13 shows the response of beam CC1 to wetting in terms of electric resistance changes. The initial resistance values are listed in the figure itself. In this beam, the wetting test has been conducted after the mechanical testing and the associate formation of cracks. The test has been conducted by wetting specific zones along the lower (tensed) face of the beam with tap water. The test has started with wetting the hairline crack region near the left support while keeping the rest of the beam dry. Then, the cracked region at the center of the beam has been wetted. Finally, the large crack formed near the right support (Figure 7) has been wetted.

Figure 14 shows the response of beam CC2 to wetting in terms of changes to the electrical resistance. The reference (initial) resistance values are also listed in the figure. Here, the wetting test is conducted before any mechanical loading. This beam is considered as a

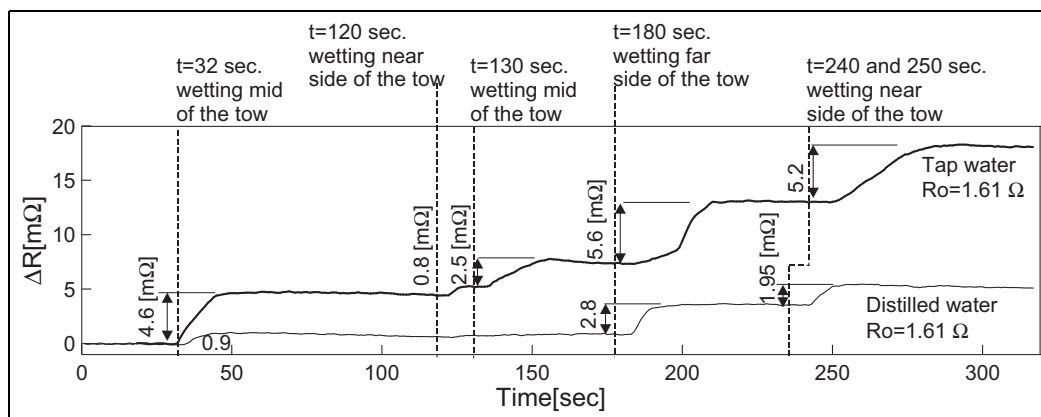


Figure 12. Resistance changes due to wetting test of carbon tow with distilled and tap water.

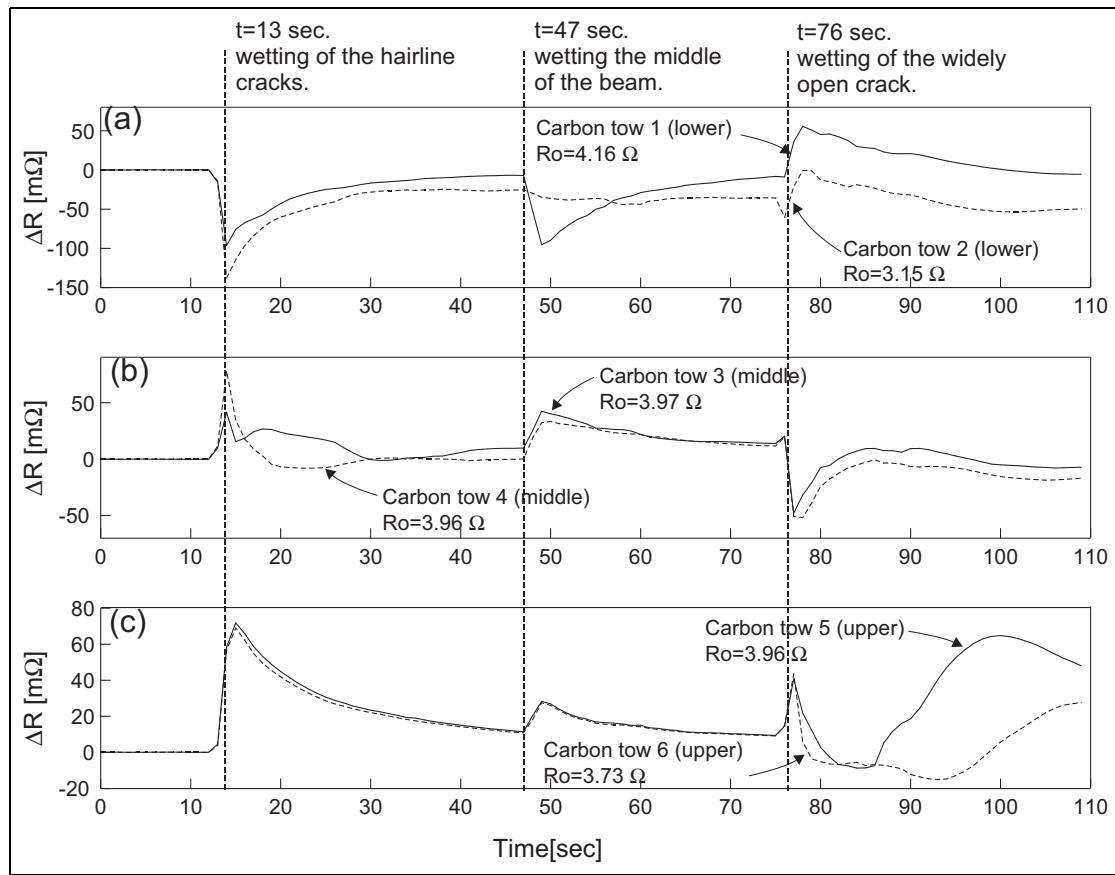


Figure 13. Resistance changes due to wetting test of cracked (preloaded) beam CC1: (a) tows No. 1 and 2, lower face; (b) tows No. 3 and 4, middle; and (c) tows No. 5 and 6, upper face.

control specimen for the wetting response of beam CC1. Since this beam was not cracked, the test included one wetting event in which the lower face of the beam has been wetted at the middle third of the span.

Figure 13 reveals that all three wetting events of the cracked beam CC1 are clearly captured by the sensory textile. The first two events, which include wetting the region with the hairline cracks near the left support at $t = 13$ s and at the middle of the beam at $t = 47$ s, are well observed in the form of significant jumps in the electrical readings. The third wetting event, which includes wetting of the widely opened crack at $t = 76$ s, is also well detected by all sensory carbon tows. These observations clearly indicate that the sensory textile effectively detects the wetting of the cracked beam.

The responses of the six carbon tows in the uncracked beam CC2 (Figure 14) reveal a total insensitivity to wetting. The wetting of this beam started at $t = 6$ s and continued till $t = 50$ s. The wetting event is not detected at all. The resistance changes that are detected in Figure 14 are 1–2 order of magnitudes smaller than the ones observed in Figure 13 in response to wetting of the cracked beam. These observations clearly indicate that the electrical response to wetting is

conditioned by the cracking of the beam. In that sense, the electrical response to wetting can be effectively used as an indicator for the cracking condition of the beam. At the same time, it can be used for the detection of the functionality of the element. If a beam is placed in a suitable wet environment, the monitoring of the electrical readings can indicate cracking of the beam. In parallel, if the beam is cracked, the monitoring of the electrical readings can indicate wetting of the beam, penetration of water, or leakage. This combination designates the glass/carbon TRC element as a multifunctional sensory one.

Conclusions

In this article, the concept of using glass/carbon fiber-based textile reinforcement for the development of a self-sensory TRC element has been examined. The study has pointed out the potential of using the hybrid glass/carbon TRC element as a multifunctional sensory and structural component and the feasibility of this approach. The structural behavior of the concrete element, reinforced with the sensory textile, reveals a satisfactory structural response in terms of the initial pre-cracked linear behavior, the post-cracking

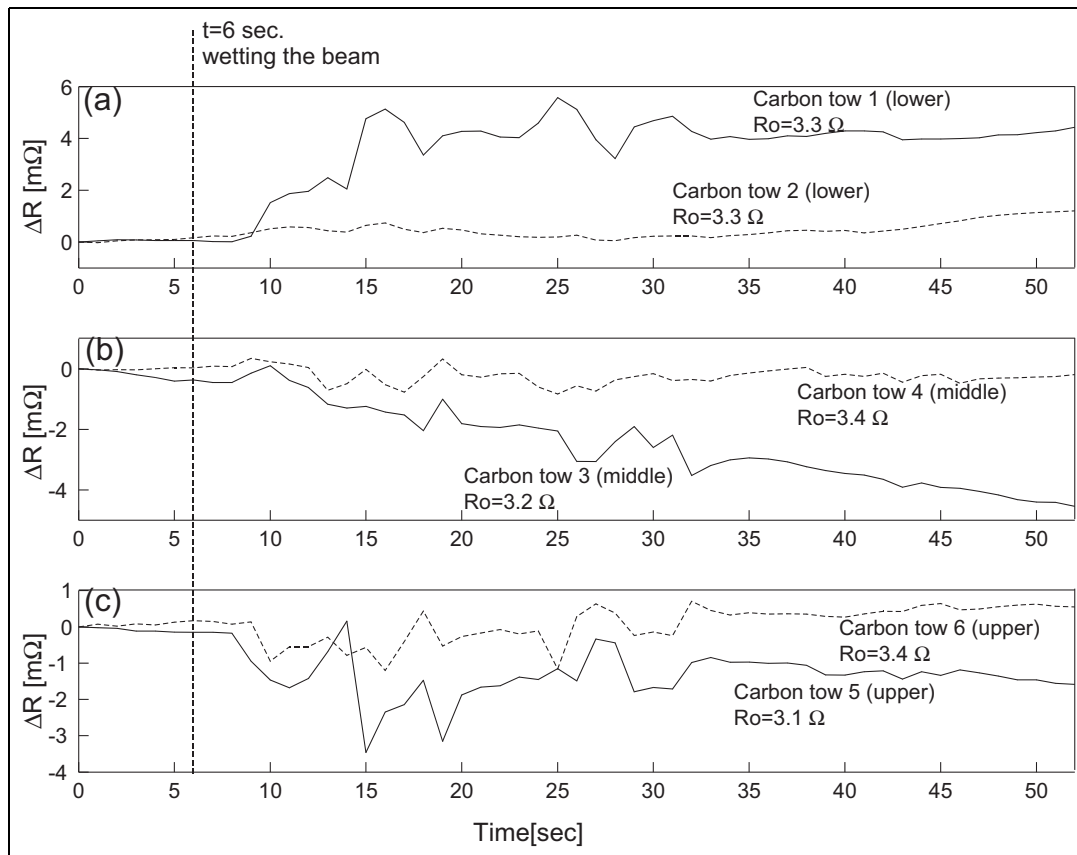


Figure 14. Resistance changes due to wetting test of un-cracked beam CC2: (a) tows No. 1 and 2, lower face; (b) tows No. 3 and 4, middle; and (c) tows No. 5 and 6, upper face.

behavior, the distribution and width of cracks, the behavior at ultimate stages, and the mode of failure. At the same time, the structural textile provides continuous electrical readings that, by means of a linear calibration, quantitatively describe and monitor the mechanical state of the structural element. This provides the TRC element with the ability to detect and monitor its structural condition. This step paves the way to a spectrum of applications of self-sensory and smart concrete structures.

The experimental study has also shown that the electrical readings of the textile provide an effective indication of wetting of the cracked TRC element. Specifically, it detects the sequential effect of wetting and cracking. This feature has two implications. First, the ability to detect cracks is particularly interesting because it reflects the structural state even after the load has been removed. Even if the duration of the load is too short to be captured by the temporal resolution of the strain monitoring system, the monitoring of the interaction with the wet environment can effectively point at the evolution of cracks. This can serve as an indicator for the residual structural state after an extreme event such as earthquake, tsunami, wind gust, impact loading, or even a terrorist sabotage. Second, the ability to detect interaction with an aqueous environment can be used to monitor the

functionality of the infrastructure. For example, it can detect leakage and thus avoid loss of drinking water in concrete water pipelines or mitigate the hazard of environmental pollution due to leakage in wastewater pipelines. At a larger urban scale, the continuous monitoring and the ability to detect failure in large-scale pipeline networks can be used for detecting regions struck by a natural or manmade disaster and for pointing at regions where the damage is most severe. This information can become helpful for guiding medical and rescue squads to the struck region.

The capabilities discussed in this article demonstrate the potential feasibility of the sensory TRC element concept. This feasibility joins the favorable features of the thin-walled high-strength TRC element and its broad spectrum of applications. Together, they take a meaningful step toward the development of efficient, sustainable, economically viable, and safe intelligent concrete structures. In order to take further steps in this direction, the investigation should be expanded to additional directions. These research directions include, but not limited to, the characterizing the reversible and irreversible components of the resistance changes; the various aspect that effect the noise in the electrical data; the coupling of the wetting and the strain effect in terms of the electrical reading; the sensitivity and the

noise of the electrical measurement with respect to the electrical scheme (two-probe versus four-probe methods); the effects of time and temperature; the electrical and mechanical interaction with adjacent steel reinforcement; and the micro-electro-mechanical processes that govern the macroscopic behavior reported here.

Acknowledgement

The authors are grateful for the help of Barak Ofir, Elhanan Yitzhak, and the technical and administrative staff of the National Building Research Institute at the Technion.

Declaration of Conflicting Interests

The authors declared no potential conflicts of interest with respect to the research, authorship, and/or publication of this article.

Funding

The author(s) disclosed receipt of the following financial support for the research, authorship, and/or publication of this article: This study was financially supported by the Umbrella Cooperation Program of the Technion – Israel Institute of Technology, RWTH, Aachen University and JULICH Forschungszentrum.

References

- Angelidis N, Wei CY and Irving PE (2004) The electrical resistance response of continuous carbon fiber composite laminates to mechanical strain. *Composites Part A: Applied Science and Manufacturing* 35: 1135–1147.
- Bakis CE, Nanni A, Terosky JA, et al. (2001) Self-monitoring, pseudo-ductile, hybrid FRP reinforcement rods for concrete applications. *Composites Science and Technology* 61: 815–823.
- Berger U, Hausding J, Cherif C, et al. (2011) Herstellungskonzepte für die Textilverstärkung mit 50 K Kohlenstoff-Filamentgarn für Bauingenieuranwendungen [Production concepts for textile reinforcements made of 50 K carbon filament yarn for civil engineering applications]. In: *New material characteristics to cover new applications needs, SEICO, SAMPE Europe international technical conference & forum*, Paris, 28–29 March.
- Chen P-W and Chung DDL (1993a) Carbon fiber reinforced concrete as an electrical contact material for smart structures. *Smart Material and Structures* 2(1): 181–188.
- Chen P-W and Chung DDL (1993b) Carbon fiber reinforced concrete for smart structures capable of non-destructive flaw detection. *Smart Material and Structures* 2(1): 22–30.
- Chen P-W and Chung DDL (1995) Carbon fiber reinforced concrete as an intrinsically smart concrete for damage assessment during dynamic loading. *Journal of the American Ceramic Society* 78(3): 816–818.
- Chung DDL (2000a) Cement-matrix composites for smart structures. *Smart Material and Structures* 9(4): 389–401.
- Chung DDL (2000b) Cement reinforced with short carbon fibers: a multifunctional material. *Composite Part B: Engineering* 31(6–7): 511–526.
- Chung DDL (2001a) Cement-based electronics. *Journal of Electroceramics* 6(1): 75–88.
- Chung DDL (2001b) Continuous carbon fiber polymer-matrix composites and their joints, studied by electrical measurements. *Polymer Composites* 22(2): 250–270.
- Chung DDL (2002) Electrical conduction behavior of cement-matrix composites. *Journal of Materials Engineering and Performance* 11: 194–204.
- Chung DDL (2003) Damage in cement-based materials, studied by electrical resistance measurement. *Materials Science & Engineering R: Reports* 52(1): 1–40.
- Chung DDL (2005) Dispersion of short fibers in cement. *Journal of Materials in Civil Engineering* 17: 379–383.
- Chung DDL (2007) Damage detection using self-sensing concepts. *Proceedings of the Institution of Mechanical Engineers, Part G: Journal of Aerospace Engineering* 221(4): 509–520.
- Chung DDL (2012) Carbon materials for structural self-sensing, electromagnetic shielding and thermal interfacing. *Carbon* 50: 3342–3353.
- Ding Y, Chen Z, Han Z, et al. (2013) Nano-carbon black and carbon fiber as conductive materials for the diagnosing of the damage of concrete beam. *Construction and Building Materials* 43: 233–241.
- EN 196-1:2005 (2005) Methods of testing cement—part 1: determination of strength, European Committee for Standardization.
- Franzke G, Engler T, Lieboldt M, et al. (2005) Doppelt hält länger. Textilverstärkte Mehrschichtrohre für Druckrohrleitungssysteme [Double layered is more durable. Textile reinforcement for multi-layered pressure pipe systems]. *Kettenwerk-Praxis* 39(2): 15–17.
- Goldfeld Y and Klar A (2013) Damage identification in reinforced concrete beams using spatially distributed strain measurements. *Journal of Structural Engineering: ASCE* 139(12): 04013013 (1–12).
- Goldfeld Y, Rabinovitch O, Quadflieg T, et al. (2014) Smart textile reinforced concrete sensory structures. In: *Proceedings of the 7th European workshop on structural health monitoring*, Nantes, 8–11 July.
- Guerrero VH, Wang S, Wen S, et al. (2002) Thermoelectric property tailoring by composite engineering. *Journal of Materials Science* 37: 4127–4136.
- Han B, Guan X and Ou J (2007) Electrode design, measuring method and data acquisition system of carbon fiber cement paste piezoresistive sensors. *Sensors and Actuators A: Physical* 135: 360–369.
- Hegger J, Golraski C and Kulas MC (2011) Schlanke Fußgängerbrücke aus Textilbeton—Sechsfeldrige Fußgängerbrücke mit einer Gesamtlänge von 97 m. *Beton- und Stahlbetonbau* 106(2): 64–71.
- Khotiaintsev S, Beltrán-Hernández A and González-Tinoco J, et al. (2013) Structural health monitoring of concrete elements with embedded arrays of optical fibers. In: *Proceedings of SPIE conference on health monitoring of structural and biological systems*, San Diego, CA, 11–14 March, vol. 8695 (Article number 869513).
- Klar A, Goldfeld Y and Chares Z (2010) Measures for identifying cracks within reinforced concrete beams using BOTDR. In: *Proceedings of the SPIE Sensors and Smart structures technologies for civil mechanical and aerospace*

- systems, San Diego, CA, 31 March, vol. 7647 (Article number 764721).
- Krebbber K, Lenke P, Liehr S, et al. (2012) Structural health monitoring by distributed fiber optic sensors embedded into technical textiles. *Beitrage: Technisches Messen* 79(7–8): 337–347.
- Lee B (2003) Review of present status of optical fiber sensors. *Optical Fiber Technology* 9: 57–79 (7–8): 337–347.
- Li H-N, Li D-S and Song G-B (2004) Recent applications of fiber optic sensors to health monitoring in civil engineering. *Engineering Structures* 26(11): 1647–1657.
- Lieboldt M, Helbig U and Engler T (2006) Textile reinforced concrete multilayer composite pipes. In: Hegger J, Bramehuber W and Will N (eds) *Proceedings of the ICTRC'2006—1st International RILEM Conference on Textile Reinforced Concrete*. Bagnaux: RILEM Publications SARL, pp. 369–378.
- McCarter WJ, Starrs G, Chrisp TM, et al. (2007) Activation and conduction in carbon fibre reinforced cement matrices. *Journal of Materials Science* 42: 2200–2203.
- Majumder M, Gangopadhyay TK, Chakraborty AK, et al. (2008) Fibre Bragg gratings in structural health monitoring—present status and applications. *Sensors and Actuators A: Physical* 147(1): 150–163.
- Meehan DG, Wang S and Chung DDL (2010) Electrical-resistance-based sending of impact damage in carbon fiber reinforced cement-based materials. *Journal of Intelligent Material Systems and Structures* 21: 84–105.
- Mei Z and Chung DDL (2000) Effects of temperature and stress on the interface between concrete and its carbon fiber epoxy-matrix composite retrofit, studied by electrical resistance measurement. *Cement and Concrete Research* 30: 799–802.
- Montanini R, De Domenico F, Freni F, et al. (2012) Structural health monitoring of reinforced concrete beams by means of embedded fiber Bragg grating sensors. In: *Proceedings of the SPIE 22nd international conference on optical fiber sensors*, Beijing, China, 15–19 October, vol. 8421 (Article number 8421AW).
- Nanni F, Ruscito L, Nad L, et al. (2009) Self-sensing nanocomposite CnP–GFRP rods as reinforcement and sensors of concrete beams. *Journal of Intelligent Material Systems and Structures* 20: 1615–1622.
- Ou J and Han B (2009) Piezoresistive cement-based strain sensors and self-sensing concrete components. *Journal of Intelligent Material Systems and Structures* 20: 329–336.
- Quadflieg T, Tomoscheit S and Gries T (2013) Humidity and strain monitoring for textile reinforced concrete. In: *Second conference on smart monitoring, assessment and rehabilitation of civil structures*, Istanbul, 9–11 September.
- Todoroki A and Yoshida J (2004) Electrical resistance change of unidirectional CFRP due to applied load. *JSME International Journal Series A* 47(3): 357–364.
- Vaidya S and Allouche EN (2011) Strain sensing of carbon fiber reinforced geopolymer concrete. *Materials and Structures* 44: 1467–1475.
- Wang D, Wang S, Chung DDL, et al. (2006) Comparison of the electrical resistance and potential techniques for the self-sensing of damage in carbon fiber polymer-matrix composites. *Journal of Intelligent Material Systems and Structures* 17: 853–860.
- Wang S and Chung DDL (1999a) Apparent negative electrical resistance in carbon fiber composites. *Composites Part B: Engineering* 30: 579–590.
- Wang S and Chung DDL (1999b) Temperature/light sensing using carbon fiber polymer-matrix composite. *Composites Part B: Engineering* 30: 591–601.
- Wang S, Shui XF and Chung DDL (1998) Early fatigue damage in carbon-fibre composites observed by electrical resistance measurement. *Journal of Materials Science* 33: 3875–3884.
- Wang X and Chung DDL (1996) Continuous carbon fiber epoxy-matrix composite as a sensor of its own strain. *Smart Materials and Structures* 5(6): 796–800.
- Wang X, Fu X and Chung DDL (1999) Strain sensing using carbon fiber. *Journal of Materials Research* 14(3): 790–802.
- Wen S and Chung DDL (1999) Piezoresistivity in continuous carbon fiber cement-matrix composite. *Cement and Concrete Research* 29: 445–449.
- Wen S and Chung DDL (2005) Strain-sensing characteristics of carbon fiber-reinforced cement. *ACI Materials Journal* 102(4): 244–248.
- Wen S and Chung DDL (2006) Self-sensing of flexural damage and strain in carbon fiber reinforced cement and effect of embedded steel reinforcing bars. *Carbon* 44: 1496–1502.
- Wen S and Chung DDL (2007) Electrical-resistance-based damage self-sensing in carbon fiber reinforced cement. *Carbon* 45: 710–716.
- Wen S and Chung DDL (2008) Effect of moisture on piezoresistivity of carbon fiber reinforced cement paste. *ACI Materials Journal* 105: 274–280.
- Wen S, Wang S and Chung DDL (1999) Carbon fiber structural composites as thermistors. *Sensors and Actuators* 78: 180–188.
- Wen S, Wang S and Chung DDL (2000) Piezoresistivity in continuous carbon fiber polymer-matrix and cement-matrix composites. *Journal of Materials Science* 35: 3669–3675.
- Xu Y and Chung DDL (2001) Silane-treated carbon fiber for reinforcing cement. *Carbon* 39: 1995–2001.
- Yang CQ and Wu ZS (2006) Self-structural health monitoring function of RC structures with HCFRP sensors. *Journal of Intelligent Material Systems and Structures* 17: 895–906.
- Zdraveva E, Gonilho-Pereira C, Figueiro R, et al. (2010) Multifunctional braided composite rods for civil engineering applications. *Advanced Materials Research* 123–125: 149–152.
- Zhu S and Chung DDL (2007) Analytical model for piezoresistivity for strain sensing in carbon fiber polymer-matrix structural composite. *Carbon* 45: 1606–1613.